DALTON
FULL PAPER

Experimental and theoretical studies of the molecular and crystal structures of trialkoxy- and chlorodialkoxy-stibanes †

Holger Fleischer,*[a] Hatice Bayram,[a] Stephan Elzner[a] and Norbert W. Mitzel[b]

[a] *Institut für Anorganische Chemie und Analytische Chemie, Universität Mainz, Duesbergweg 10–14, D-55099 Mainz, Germany. E-mail: fleische@mail.uni-mainz.de*
[b] *Anorganisch-chemisches Institut, Technische Universität München, Lichtenbergstraße 4, 85747 Garching, Germany*

Received 2nd October 2000, Accepted 20th December 2000
First published as an Advance Article on the web 30th January 2001

The molecular structures of triisopropoxystibane, $Sb(O^iPr)_3$, and chlorodiisopropoxystibane, $SbCl(O^iPr)_2$, were determined in the solid state by single crystal X-ray diffraction. $Sb(O^iPr)_3$ forms discrete centrosymmetric dimers in the solid state *via* Sb · · · O–Sb interactions, leading to pseudo trigonal bipyramidal configurations of the four co-ordinate Sb atoms, while $SbCl(O^iPr)_2$ forms chains *via* Sb · · · O–Sb and Sb · · · Cl–Sb bridges, resulting in five-co-ordinate Sb atoms with pseudo octahedral configurations. Comparison of the solid state structures and the density functional optimized molecular structures of $Sb(OMe)_3$, $SbCl(OMe)_2$ and their dimers revealed a steady increase of the average Sb–O bond lengths with the co-ordination number of Sb, and mutual *trans* effects of the ligands. Standard enthalpies of dimer formation from density functional calculations are −23.8 and −69.7 kJ mol^{-1} for $[Sb_2(\mu\text{-}OMe)_2(OMe)_4]$ and $[Sb_2Cl_2(\mu\text{-}OMe)_2(OMe)_2]$, respectively, and −42.7 kJ mol^{-1} for $[Sb_2(\mu\text{-}Cl)_2(OMe)_4]$. A natural bond orbital analysis reveals that n(O)–σ*(Sb–O) and n(O)–σ*(Sb–Cl) interactions are the main contributions to the inter-monomer bonding in the O-bridged dimers, of $Sb(OMe)_3$ and $SbCl(OMe)_2$, respectively, while n(Cl)–σ*(Sb–O) plays no significant role in the Cl-bridged dimer of $SbCl(OMe)_2$. IR and Raman spectra of $Sb(O^iPr)_3$ indicated molecular association in the solid and liquid phase, but dissociation into monomers in non-polar solvents.

Introduction

There is a variety of modes of intermolecular interactions and co-ordination in the solid state structures of alkoxy- and halogeno-stibanes. $SbCl_3$ forms a three dimensional net *via* Sb–Cl · · · Sb bridges and the co-ordination of Sb is best described as a twofold capped trigonal prism, with a stereochemically active lone pair.[1,2] The structures of some alkoxy- and alkoxy-halogeno-stibanes and -bismuthanes in the solid state and in solution were investigated by Schmidt and others. They found ligand exchange[3] and aggregation of $SbX_n(OR)_{3-n}$ in solution (X = Cl or Br, n = 0, 1 or 2) and strong intermolecular interactions in the solid state for $Sb(OMe)_3$,[4] $SbCl(OEt)_2$,[5] $SbCl_2(OEt)$,[5] $SbCl_2(OEt)\cdot NHMe_2$,[6] $Sb(OMe)_5$,[7] $SbCl_4(OMe)$,[8] $SbCl_4(OEt)$,[9] $SbBr_2Me(OMe)_2$,[10] and $Bi[OCH(CF_3)_2]_3\cdot$thf [11] *via* Sb–Cl · · · Sb, Sb–O · · · Sb and Bi–O · · · Bi bridges.

While pentavalent antimony compounds form discrete dimers (Fig. 1b), dimeric and polymeric structures are found with trivalent Sb and Bi (Fig. 1a). Among the alkoxides of the p-block elements, the methoxides tend to adopt polymeric structures, while *tert*-butoxides, due to the bulkiness of the ligands, are mostly monomeric.[12] Isopropoxides are in between the two cases in terms of steric demand and their structural chemistry offers several modes of aggregation, *e.g.* $Si(O^iPr)_4$ is monomeric[13] while $Al(O^iPr)_3$ exhibits a tetrameric structure.[14]

Recently, Landrum and Hoffmann published a survey of solid state structures comprising secondary bonds between halogen atoms and the heavier Group 15 elements.[15] They stated that, in contrast to earlier reports,[16] secondary bonds may well form towards the lone pair of a central atom, *e.g.* Sb^{III}. We were thus interested to have a closer look at the intermolecular interactions of alkoxy- and chloroalkoxy-stibanes by means of experimental and theoretical methods and to study the influence of R on the aggregation of $Sb(OR)_3$.

Experimental and theoretical procedures

General procedures

All operations involving $SbCl_3$, $Sb(O^iPr)_3$ and $SbCl(O^iPr)_2$ were carried out under an inert gas atmosphere or in vacuum, using carefully dried glassware and solvents purified according to standard procedures. NMR: Bruker DRX 400 spectrometer, $B_1(^1H)$ = 400.0 MHz, $B_1(^{13}C)$ = 100.577 MHz. Standard: TMS (^1H, ^{13}C). IR: Mattson Galaxy 2030 FTIR spectrometer, resolution 4 cm^{-1}, CsI pellets, range 4000–200 cm^{-1}. Raman: DILOR XY 800 spectrometer, excitation at 633 nm. CH analysis was performed with an Elemental Vario EL2 instrument. $Sb(O^iPr)_3$ and $SbCl(O^iPr)_2$ were prepared according to literature procedures.[17,3] Identity and purity was established by melting point, CH analysis and ^1H NMR spectroscopy.

Crystal structure determination

A single crystal of $Sb(O^iPr)_3$ was grown *in situ* by slowly cooling the melt in a sealed capillary below the melting point of 4 °C after generation of a suitable seed crystal by shock freezing and microscale zone refinement slightly below the melting point. Single crystals of $SbCl(O^iPr)_2$ were obtained by vacuum sublimation (1 mmHg/40 °C) and a selected one was mounted under inert perfluoropolyether. Data collection was undertaken on a CAD4 diffractometer using Mo-Kα radiation (λ = 71.073 pm). Details of the data collection and refinement are listed in Table 1. The structure solutions were performed with direct methods, the refinements based on F^2 and carried out with the SHELXTL 5.01 program.[18] Non-hydrogen atoms were refined with anisotropic displacement parameters. Hydrogen atoms

† Electronic supplementary information (ESI) available: archive sections of GAUSSIAN94 output. See http://www.rsc.org/suppdata/dt/b0/b007926j/

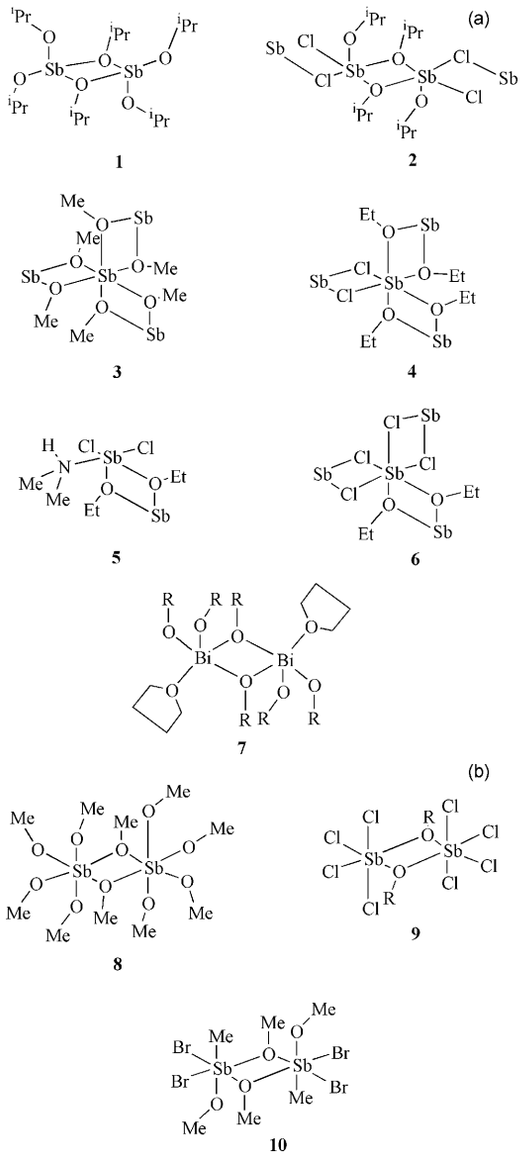

Fig. 1 Structural formulae of several trivalent (a) and pentavalent (b) alkoxy-stibanes and -bismuthanes discussed in the present paper, showing the co-ordination of the central atoms and modes of aggregation: $Sb(O^iPr)_3$ **1**, $SbCl(O^iPr)_2$ **2**, $Sb(OMe)_3$ **3**, $SbCl(OEt)_2$ **4**, $SbCl_2(OEt)\cdot NHMe_2$ **5**, $SbCl_2(OEt)$ **6**, $Bi[OCH(CF_3)_2]_3\cdot thf$ **7**, $Sb(OMe)_5$ **8**, $SbCl_4(OR)$ (R = Me or Et) **9** and $SbBr_2Me(OMe)_2$ **10**.

were placed in calculated positions and included in the refinement with a riding model.

CCDC reference number 186/2306.

See http://www.rsc.org/suppdata/dt/b0/b007926j/ for crystallographic files in .cif format.

Theoretical methods

The density functional calculations were performed on various servers of the Zentrum für Datenverarbeitung, Universität Mainz, using the GAUSSIAN 94 software package.[19] The geometries of all molecules were fully optimized using an effective core double zeta valence basis set according to Hay and Wadt[20] augmented by appropriate polarization functions for Sb, Cl (with exponents according to Höllwarth *et al.*[21]), O and C (exponents 0.85 and 0.50, respectively) and density functional theory[22] employing a combination of local, gradient-corrected, and exact exchange functionals according to the prescription of Becke[23] and the gradient-corrected correlation functional of Lee *et al.*[24] [B3LYP/LANL2DZP]. $Sb(OMe)_3$ was restricted to C_3 symmetry, while $SbCl(OMe)_2$ was optimized without a symmetry constraint. The dimeric forms, $[Sb_2(\mu\text{-}OMe)_2(OMe)_4]$, $[Sb_2Cl_2(\mu\text{-}OMe)_2(OMe)_2]$ and $[Sb_2(\mu\text{-}Cl)_2(OMe)_4]$, were restricted to C_i symmetry. Vibrational frequencies were obtained numerically from first derivatives of the potential energy. The thermochemical data for dimer formation from the monomers were corrected for the basis set superposition error, estimated with counterpoise calculations based on the B3LYP/LANL2DZP geometry.[25,26] An analysis of the bonding situation in the dimeric species was performed using a natural bond orbital (NBO) basis.[27,28]

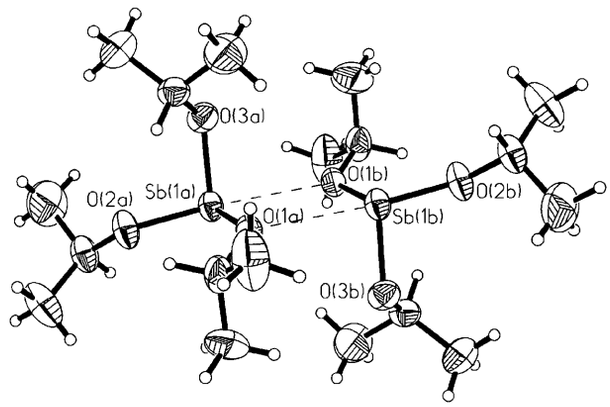

Fig. 2 Molecular structure of the $Sb(O^iPr)_3$ dimer in the solid state. Displacement ellipsoids are at the 50% probability level.

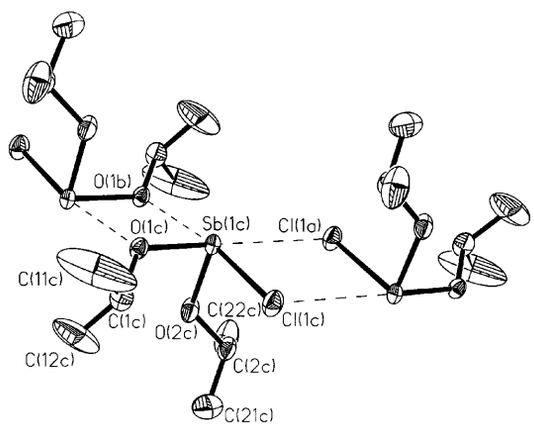

Fig. 3 Fragment of the solid state structure of $SbCl(O^iPr)_2$. Hydrogen atoms are omitted for clarity. Displacement ellipsoids as in Fig. 2.

Results and discussion

$Sb(O^iPr)_3$ crystallizes by forming discrete molecular dimers with a co-ordination number $CN_{Sb} = 4$ and a pseudo trigonal bipyramidal configuration of the Sb atom, instead of building three-dimensional networks *via* Sb···O–Sb bridges, as was found for $Sb(OMe)_3$.[4] Solid $SbCl(O^iPr)_2$ exhibits five-co-ordinate Sb atoms with a pseudo octahedral configuration, in contrast to $SbCl(OEt)_2$ and $SbCl_2(OEt)$,[5] that contain six-co-ordinate Sb atoms in the solid state. The stereochemical activity of the lone pair at the Sb atom is inferred from the values of the bonding angles and can be seen in Figs. 2 and 3. $Sb(O^iPr)_3$ and $SbCl(O^iPr)_2$ both obey all of Alcock's three rules for secondary interactions:[16] The geometry of the primary Sb–Cl and Sb–O bonds is determined by the VSEPR rules, all secondary Sb···O and Sb···Cl bonds are more of less opposite primary ones and no secondary bonds point toward the lone pair of Sb^{III}.

The Sb···O distances are significantly shorter in the solid state structures of the chlorodialkoxystibanes than in the solid state structure of the trialkoxystibanes (see Tables 2, 3 and 4). Sb···O in $SbCl(O^iPr)_2$ and the shorter of the two Sb···O

contacts in $SbCl(OEt)_2$ exhibit about the same lengths. Accordingly, the lengths of the Sb–Cl bonds in *trans* position to these Sb···O contacts are nearly equal as well. It is inferred that a Cl atom in *trans* position to an Sb···O contact allows for a stronger interaction than an O atom in *trans* position does (See below for calculated energies of interaction).

Regarding the structural parameters given in Tables 2, 3 and 4, a slight increase of the average covalent Sb–O bond lengths is observed, if CN_{Sb} is increased.[29] The average Sb–O distances for the trialkoxystibanes increase from 195.8 pm for monomeric $Sb(OMe)_3$ ($CN_{Sb} = 3$) to 200.1 pm for $Sb(OMe)_3$ in the solid state ($CN_{Sb} = 6$), and the average Sb–O distances for the chlorodialkoxystibanes from 193.5 pm for monomeric $SbCl(OMe)_2$ ($CN_{Sb} = 3$) to 199.6 pm for $SbCl(OEt)_2$ in the solid state ($CN_{Sb} = 6$). Having a constant CN_{Sb}, the average Sb–O bond lengths are shorter for $SbCl(OR)_2$ than for $Sb(OR)_3$ compounds. The endocyclic Sb–O bonds were found to be longer than the exocyclic ones and Sb–O bonds in *trans* position to short Sb···O contacts are longer than those in *trans* position to longer Sb···O contacts or the lone pair of Sb, in accordance with what is expected.

Sb–Cl bonds are slightly shorter in the DF optimized molecular structures ($CN_{Sb} = 3$ or 4, see Fig. 4) than in the solid state structures ($CN_{Sb} = 5$ or 6). They are similar for $SbCl(OEt)_2$ and $SbCl(O^iPr)_2$; the Sb···Cl distances are slightly shorter for the latter. Comparision of the DF optimized geometric parameters of $[Sb_2(\mu\text{-}Cl)_2(OMe)_4]$ and $SbCl(OMe)_2$ reveal an increase of the Sb–Cl bond length on dimerization, as expected. The

Table 1 Crystal and structure refinement data for $Sb(O^iPr)_3$ and $SbCl(O^iPr)_2$

	$Sb(O^iPr)_3$	$SbCl(O^iPr)_2$
Empirical formula	$C_9H_{21}O_3Sb$	$C_6H_{14}ClO_2Sb$
Formal weight/g mol^{-1}	299.01	275.37
T/K	173(2)	143(2)
Crystal system	Orthorhombic	Monoclinic
Space group	*Pbca*	*C*2/*c*
a/nm	1.54207(14)	1.7035(2)
b/nm	0.92306(7)	1.4884(2)
c/nm	1.85641(16)	0.8065(1)
β/°		93.08(1)
V/nm^3	2.6425(4)	2.0419(4)
Z	8	8
μ/mm^{-1}	2.069	2.915
Reflections collected/ unique	7223/3858 [*R*(int) = 0.0448]	2394/2220 [*R*(int) = 0.0080]
*R*1, *wR2* [$I > 2\sigma(I)$]	0.0320, 0.0815	0.0208, 0.0506
all data	0.0509, 0.0881	0.0256, 0.0529

Table 2 Selected structural parameters (atomic distances in ppm, angles in degrees) from the single crystal XRD structure of $Sb(O^iPr)_3$

Sb(1A)–O(1A)	197.3(2)	O(1A)–Sb(1A)–O(3A)	95.3(1)
Sb(1A)···O(1B)	296.6(2)	O(2A)–Sb(A)–O(3A)	95.1(1)
Sb(1A)–O(2A)	197.6(2)	O(2A)–Sb(1A)···O(1B)	160.9(1)
Sb(1A)–O(3A)	193.5(2)	C(2A)–O(1A)–Sb(1A)	124.1(2)
O(1A)–C(2A)	144.0(3)	C(1A)–O(2A)–Sb(1A)	119.2(1)
O(2A)–C(1A)	142.2(3)	C(3A)–O(3A)–Sb(1A)	121.7(2)
O(3A)–C(3A)	143.0(3)	O(2A)–C(1A)–C(11A)	110.2(3)
C(1A)–C(11A)	150.2(5)	O(2A)–C(1A)–C(12A)	107.9(2)
C(1A)–C(12A)	150.6(4)	C(11A)–C(1A)–C(12A)	112.0(3)
C(2A)–C(21A)	149.4(5)	O(1A)–C(2A)–C(21A)	109.4(3)
C(2A)–C(22A)	151.2(5)	O(1A)–C(2A)–C(22A)	106.4(2)
C(3A)–C(31A)	149.8(4)	C(21A)–C(2A)–C(22A)	114.5(4)
C(3A)–C(32A)	150.9(4)	O(3A)–C(3A)–C(31A)	108.7(2)
		O(3A)–C(3A)–C(32A)	108.7(2)
O(1A)–Sb(1A)–O(2A)	91.2(1)	C(31A)–C(3A)–C(32A)	112.4(3)

Table 3 Selected structural parameters (atomic distances in pm, angles in degrees) from the single crystal XRD structure of $SbCl(O^iPr)_2$

Sb(1C)–O(1C)	200.1(2)	Sb(1C)–O(1C)···Sb(1B)	108.8(1)
Sb(1C)···O(1B)	239.4(2)	O(1C)–Sb(1C)–Cl(1C)	94.3(1)
Sb(1C)–O(2C)	193.5(2)	O(2C)–Sb(1C)–Cl(1C)	93.0(1)
Sb(1C)–Cl(1C)	249.6(1)	O(1B)···Sb(1C)–Cl(1C)	165.5(1)
Sb(1C)···Cl(1A)	348.4(1)	Cl(1A)···Sb(1C)–O(1C)	178.1(1)
O(1C)–C(1C)	147.0(3)	Cl(1A)···Sb(1C)–O(2C)	90.7(1)
O(2C)–C(2C)	143.4(3)	Cl(1A)···Sb(1C)–Cl(1C)	84.1(1)
C(1C)–C(11C)	147.3(6)	C(1C)–O(1C)–Sb(1C)	125.0(2)
C(1C)–C(12C)	148.5(6)_	C(2C)–O(2C)–Sb(1C)	124.9(2)
C(2C)–C(21C)	151.1(5)	O(1C)–C(1C)–C(11C)	108.0(3)
C(1C)–C(22C)	149.4(5)	O(1C)–C(1C)–C(12C)	110.3(3)
		C(11C)–C(1C)–C(12C)	110.9(4)
O(1C)–Sb(1C)–O(2C)	90.3(1)	O(2C)–C(2C)–C(21C)	107.2(3)
O(1C)–Sb(1C)···O(1B)	71.3(1)	O(2C)–C(2C)–C(22C)	108.9(3)
O(2C)–Sb(1C)···O(1B)	87.0(1)	C(21C)–C(2C)–C(22C)	112.9(3)

Table 4 Selected structural parameters of $Sb(OMe)_3$ and $SbCl(OEt)_2$ from single crystal XRD experiments,[a] and of $Sb(OMe)_3$,[b] $SbCl(OMe)_2$, $[Sb_2(\mu\text{-}OMe)_2(OMe)_4]$ **A**, $[Sb_2Cl_2(\mu\text{-}OMe)_2(OMe)_2]$ **B** and $[Sb_2(\mu\text{-}Cl)_2(OMe)_4]$ **C** from DF geometry optimizations[c]

	$Sb(OMe)_3$ XRD	$SbCl(OEt)_2$ XRD	$SbCl(OMe)_2$ DF	**A** DF	**B** DF	**C** DF
r(Sb–O)	198.6(6)	196.6(4)	192.3	195.3	194.0	192.5
	200.4(9)	202.6(5)	194.6	199.4	203.3	195.4
	201.2(8)			201.3		
r(Sb···O)	256.4(10)	240.0(4)		252.9	245.7	
	288.6(7)	295.6(5)				
	300.3(7)					
r(Sb–Cl)		249.4(2)	247.7		246.5	246.3
r(Sb···Cl)		353.8(2)				360.7
α(O–Sb···O^{tr})[d]	155.9(3)	166.3(2)		155.8		
	157.0(2)					
	160.4(3)					
α(Cl–Sb···O^{tr})[d]		154.1(1)			161.7	
α(O–Sb···Cl^{tr})[d]		161.5(1)				172.2

[a] XRD structures of $Sb(OMe)_3$ and $SbCl(OEt)_2$ were taken from references 4 and 5, respectively. [b] *r*(Sb–O) = 195.8 pm for $Sb(OMe)_3$. [c] XRD values represent r_a, DF values r_e structures. [d] "tr" refers to an O or Cl atom in *trans* position to the primary Sb–O or Sb–Cl bond.

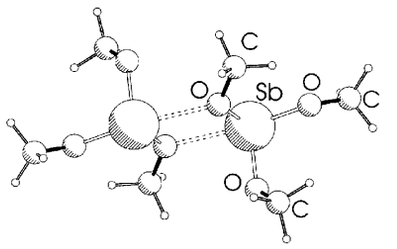

1

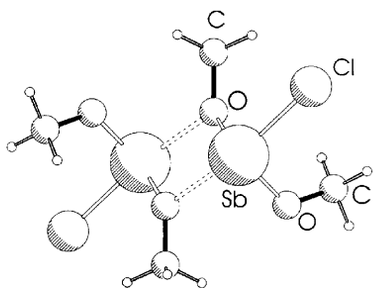

2

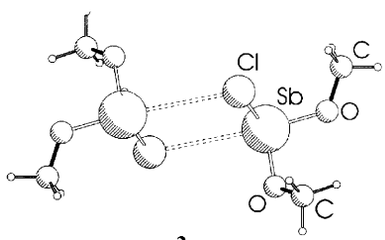

3

Fig. 4 B3LYP/LANL2DZP optimized geometries of $[Sb_2(\mu\text{-}OMe)_2(OMe)_4]$ **1**, $[Sb_2Cl_2(\mu\text{-}OMe)_2(OMe)_2]$ **2** and $[Sb_2(\mu\text{-}Cl)_2(OMe)_4]$ **3**.

lengthening of the Sb–O bonds by Sb · · · Cl bonds *trans* to them is much less pronounced than the effect of Sb · · · O bonds on a Sb–Cl bond in *trans* position. This difference can be explained by an analysis of the natural orbital interaction (see below). The DF optimized Sb · · · Cl bond is found to be slightly longer than the experimental ones, but reflects the magnitude of difference to the length of the Sb–Cl bond very well.

Judged by the angles between primary and secondary bonds in *trans* position to each other, distortions from an ideal geometry, *i.e.* $a(X\text{–}Sb\cdots X') = 180.0°$, are more pronounced in the solid state structures with higher CN_{Sb} (*i.e.* $Sb(OMe)_3$ and $SbCl(OEt)_2$) than in those with lower CN_{Sb} (*i.e.* $Sb(O^iPr)_3$ and $SbCl(O^iPr)_2$). $a(X\text{–}Sb\cdots X')$ is found to be more narrow in the *ab initio* optimized structures of $[Sb_2(\mu\text{-}OMe)_2(OMe)_4]$, $[Sb_2Cl_2(\mu\text{-}OMe)_2(OMe)_2]$ and $[Sb_2(\mu\text{-}Cl)_2(OMe)_4]$ than in the solid state structures of $Sb(O^iPr)_3$ and $SbCl(O^iPr)_2$.

B3LYP/LANL2DZP thermochemical calculations of the dimerization reactions (1), (2) and (3) suggest that all proceed exothermically, but only $SbCl(OMe)_2$ leads to dimers stable towards dissociation under normal conditions [$\Delta H^{298} = -23.8$, -69.7 and -42.7 kJ mol^{-1} and $\Delta G^{298} = +10.2$, -15.9 and -5.2 kJ mol^{-1}, for reactions (1), (2) and (3), respectively.].[30]

$$2\ Sb(OMe)_3 \longrightarrow [Sb_2(\mu\text{-}OMe)_2(OMe)_4] \quad (1)$$

$$2\ SbCl(OMe)_2 \longrightarrow [Sb_2Cl_2(\mu\text{-}OMe)_2(OMe)_2] \quad (2)$$

$$2\ SbCl(OMe)_2 \longrightarrow [Sb_2(\mu\text{-}Cl)_2(OMe)_4] \quad (3)$$

An NBO analysis of the interaction between the monomeric units in the dimers revealed n(O)–σ*(Sb–O) and n(O)–σ*(Sb–Cl) to be the major contributions to the dimerization of $Sb(OMe)_3$ and $SbCl(OMe)_2$ to $[Sb_2(\mu\text{-}OMe)_2(OMe)_4]$ and $[Sb_2Cl_2(\mu\text{-}OMe)_2(OMe)_2]$, respectively. The n(Cl)–σ*(Sb–O) interaction in $[Sb_2(\mu\text{-}Cl)_2(OMe)_4]$ was found to play only a minor role. These differences can be understood by a closer look at the factors that influence these energies (Table 5). The orbital interaction energies are proportional to the square of the respective Fock matrix elements, $\langle\varphi|\mathbf{F}|\varphi'\rangle$, which can be considered as a measure of the effective overlap of the orbitals, with φ = n(O) or n(Cl) and φ' = σ*(Sb–O) or σ*(Sb–Cl). $\langle\varphi|\mathbf{F}|\varphi'\rangle$ is rather big for n(O)–σ*(Sb–Cl) and n(O)–σ*(Sb–O), but considerably smaller for n(Cl)–σ*(Sb–O). The interaction energies are furthermore inversely proportional to the energy difference of the respective orbitals, ΔE_o. ΔE_o is more favorable for n(Cl)–σ*(Sb–O) than for n(O)–σ*(Sb–Cl) or n(O)–σ*(Sb–O), but that cannot compensate the lack in $\langle\varphi|\mathbf{F}|\varphi'\rangle^2$.

Table 5 Results from a B3LYP/LANL2DZP natural bond orbital analysis of $[Sb_2(\mu\text{-}OMe)_2(OMe)_4]$ **A**, $[Sb_2Cl_2(\mu\text{-}OMe)_2(OMe)_2]$ **B** and $[Sb_2(\mu\text{-}Cl)_2(OMe)_4]$ **C**

	A	B	C
q(Sb) [a]	2.02	1.86	1.83
$q(O^{br})$ [a]	−0.99	−1.01	—
$q_{av}(O^t)$ [a]	−1.01	−0.98	−0.97
q(Cl) [a]	—	−0.56	−0.56
n(E)–σ*(Sb–E′) [b]	43.1	71.2	11.9
ΔE_o [c]	0.64	0.58	0.41
$\langle\varphi\|\mathbf{F}\|\varphi'\rangle$ [d]	0.073	0.089	0.031

[a] Natural atomic charges in au. [b] Energy of orbital interaction in kJ mol^{-1}. [c] Energy difference between n(E) and σ*(Sb–E′), given in au E, E′ = O, Cl. [d] Fock matrix element between n(E) and σ*(Sb–E′) in au. See also text.

The thermochemistry of reaction (1) implies a nearly complete dissociation of $[Sb_2(\mu\text{-}OMe)_2(OMe)_4]$ in a non-polar environment at room temperature. As $Sb(OMe)_3$ neither forms discrete dimers in the solid state, nor dissolves in non-polar solvents, we probed the dissociation of the $Sb(O^iPr)_3$ dimer instead, by recording IR spectra of the compound in the solid and liquid state and Raman spectra of the liquid compound and its solutions in CCl_4 and cyclohexane. Both solvents are non-polar, but CCl_4 is much more polarizable and may form local dipole interactions.

The IR spectrum of $Sb(O^iPr)_3$ does not differ much between the liquid and solid phase. This implies that the dimeric structure shown to exist in the solid state is kept intact on melting. In accordance with the solid state structure of $Sb(O^iPr)_3$ that exhibits one short and two long Sb–O bonds, there is one ν(Sb–O) band at higher and two at lower frequencies, which exhibit about the same wavenumbers for the two phases (see Table 6). The Raman spectra of $Sb(O^iPr)_3$ solutions either in CCl_4 or in C_6H_{12} solution exhibit only a single band in the ν(Sb–O) region and hence dissociation into monomers is inferred, in accordance with the calculated thermochemistry of $[Sb_2(\mu\text{-}OMe)_2(OMe)_4]$. Hence on melting of $Sb(O^iPr)_3$ only weak bonds between the dimers have to be broken, while the strong Sb · · · O interactions are kept.

Conclusion

Judged by the lengths of the secondary Sb · · · O bonds and by density functional thermochemical calculations, $SbCl(O^iPr)_2$ is a stronger Lewis acid than $Sb(O^iPr)_3$ and oxygen bridges between two antimony centers are stronger than their chloride analogues. The sterically more demanding O^iPr ligands cause a reduction of the co-ordination number of antimony, CN_{Sb}, in $Sb(O^iPr)_3$ ($CN_{Sb} = 4$) and in $SbCl(O^iPr)_2$ ($CN_{Sb} = 5$) compared to $CN_{Sb} = 6$ in $Sb(OMe)_3$ and $SbCl(OEt)_2$. Primary and secondary Sb–X bonds (X = O or Cl) influence each other *via trans* effects, the main reasons for which are n(O)–σ*(Sb–X) interactions. Dimers of $Sb(O^iPr)_3$ exist in the solid and liquid state, and the rather low melting point of $Sb(O^iPr)_3$ (4 °C)

Table 6 Experimental IR and Raman bands of (a) $Sb(O^iPr)_3$ and (b) $SbCl(O^iPr)_2$[a]

(a)	IR, liq.	IR, solid	Raman, liq.	Raman, CCl_4 soln.	Raman, C_6H_{12} soln.	Assignment[b]
				614	613	ν(Sb–O) A[c]
	615vs[d]	617vs				ν(Sb–O^t) A_u[e]
			614			ν(Sb–O^t) A_g[e]
	489w					ν(Sb–O^t) A_u[e]
			495			ν(Sb–O^t) A_g[e]
	425s	425s				ν(Sb–O^b) A_u[e]
			423			ν(Sb–O^b) A_g[e]

(b)	IR	Raman	Assignment
	542vs		ν_{asym}(Sb–O^t)[f]
		518.0m	ν_{sym}(Sb–O^t)[f]
		435.2s	ν_{sym}(Sb–O^b)[f]
		256.9s	ν_{sym}(Sb–Cl)[f]

[a] Bands were assigned with the support of B3LYP/LANL2DZP vibrational frequencies of $[Sb_2(\mu\text{-}OMe)_2(OMe)_4]$ and $[Sb_2Cl_2(\mu\text{-}OMe)_2(OMe)_2]$. Modes given do not represent pure ν(Sb–O) or ν(Sb–Cl) motions, but contain contributions from skeletal motions of the lighter elements. [b] Capital letters give the irreducible representation of the mode. [c] Mode of monomeric $Sb(O^iPr)_3$. [d] Brill *et al.* reported 610 cm^{-1}.[31] [e] Mode of dimeric $[Sb(O^iPr)_3]_2$. [f] Mode of $[Sb_2Cl_2(\mu\text{-}O^iPr)_2(O^iPr)_2]$.

compared to that of $Sb(OMe)_3$ (121 °C) is attributed to the absence of significant interactions between the dimers.

Acknowledgements

H. F. thanks the Fonds der Chemischen Industrie for financial support.

References

1 A. Lipka, *Acta Crystallogr.*, *Sect. B*, 1979, **35**, 3020.
2 Throughout the paper, a single dash is used for bonds called primary or covalent and triple dots for bonds called secondary or dative.
3 R. Greiner, B. Detampel and A. Schmidt, *Monatsh. Chem.*, 1993, **124**, 827.
4 U. Ensinger, W. Schwarz, B. Schrutz, K. Sommer and A. Schmidt, *Z. Anorg. Allg. Chem.*, 1987, **544**, 181.
5 G. E. Binder, W. Schwarz, W. Rozdzinski and A. Schmidt, *Z. Anorg. Allg. Chem.*, 1980, **471**, 121.
6 A. J. Edwards, N. E. Leadbeater, M. A. Paver, P. R. Raithby, C. A. Russell and D. S. Wright, *J. Chem. Soc.*, *Dalton Trans.*, 1994, 1479.
7 N. Temple, W. Schwarz and J. Weidlein, *Z. Anorg. Allg. Chem.*, 1981, **474**, 157.
8 H. Preiss, *Z. Anorg. Allg. Chem.*, 1971, **380**, 65.
9 H. Preiss, *Z. Anorg. Allg. Chem.*, 1968, **362**, 24.
10 M. Wieber, J. Walz and C. Burschka, *Z. Anorg. Allg. Chem.*, 1990, **585**, 65.
11 C. M. Jones, M. D. Burkart and K. H. Whitmire, *Angew. Chem.*, 1992, **104**, 466; C. M. Jones, M. D. Burkart and K. H. Whitmire, *Angew. Chem.*, *Int. Ed. Engl.*, 1992, **31**, 451.
12 D. C. Bradley, R. C. Mehrotra and D. P. Gaur, *Metal Alkoxides*, Academic Press, London, New York, San Francisco, 1978 and literature cited therein.
13 N. W. Mitzel, A. J. Blake and D. W. H. Rankin, *J. Am. Chem. Soc.*, 1997, **119**, 4143.
14 K. Folting, W. E. Streib, K. G. Caulton, O. Poncelet and L. G. Hubert-Pfalzgraf, *Polyhedron*, 1991, **10**, 1639.
15 G. A. Landrum and R. Hoffmann, *Angew. Chem.*, 1998, **110**, 1989; G. A. Landrum and R. Hoffmann, *Angew. Chem.*, *Int. Ed. Engl.*, 1998, **37**, 1887.
16 N. W. Alcock, *Adv. Inorg. Radiochem.*, 1972, **15**, 1.
17 H. Meerwein and T. Bersin, *Liebigs Ann. Chem.*, 1929, **476**, 139.
18 SHELXTL 5.01, Siemens Analytical X-Ray Instrumentation Inc., Madison, WI, 1995.
19 GAUSSIAN 94, Revision E.2, M. J. Frisch, G. W. Trucks, H. B. Schlegel, P. M. W. Gill, B. G. Johnson, M. A. Robb, J. R. Cheeseman, T. Keith, G. A. Petersson, J. A. Montgomery, K. Raghavachari, M. A. Al-Laham, V. G. Zakrzewski, J. V. Ortiz, J. B. Foresman, J. Cioslowski, B. B. Stefanov, A. Nanayakkara, M. Challacombe, C. Y. Peng, P. Y. Ayala, W. Chen, M. W. Wong, J. L. Andres, E. S. Replogle, R. Gomperts, R. L. Martin, D. J. Fox, J. S. Binkley, D. J. Defrees, J. Baker, J. P. Stewart, M. Head-Gordon, C. Gonzalez and J. A. Pople, Gaussian, Inc., Pittsburgh, PA, 1995.
20 W. R. Wadt and P. J. Hay, *J. Chem. Phys.*, 1985, **82**, 284.
21 A. Höllwarth, M. Böhme, S. Dapprich, A. W. Ehlers, A. Gobbi, V. Jonas, K. F. Köhler, R. Stegmann, A. Veldkamp and G. Frenking, *Chem. Phys. Lett.*, 1993, **208**, 237.
22 R. G. Parr and W. Yang, *Density-Functional Theory of Atoms and Molecules*, Oxford University Press, 1989.
23 A. D. Becke, *J. Chem. Phys.*, 1993, **98**, 5648.
24 C. Lee, W. Yang and R. G. Parr, *Phys. Rev. B*, 1988, **37**, 785.
25 S. F. Boys and F. Bernardi, *Mol. Phys.*, 1970, **19**, 553.
26 D. W. Schwenke and D. G. Truhlar, *J. Chem. Phys.*, 1985, **82**, 2418.
27 A. E. Reed, R. B. Weinstock and F. Weinhold, *J. Chem. Phys.*, 1985, **83**, 735.
28 A. E. Reed, L. A. Curtiss and F. Weinhold, *Chem. Rev.*, 1988, **88**, 899.
29 We are aware that r_α structures from XRD experiments and r_e structures from DF calculations are compared here, but the effects discussed are bigger than the usual differences between r_α and r_e bond lengths. It has been established for weak secondary bonds to silicon that the interatomic distances are bigger in the isolated molecule than in the solid state, and that B3LYP optimizations tend slightly to overestimate these distances (H. Fleischer, *Eur. J. Inorg. Chem.*, 2001, 393).
30 No experimental data with which the B3LYP/LANL2DZP thermochemical values could be compared, are available, and calculations at the theoretically more sophisticated MP2 level were beyond the computational limits for the molecules dealt with here. For $Sb(OH)_3$, anyhow, MP2/LANL2DZP suggests a more exothermic dimerization ($\Delta E = -75.5$ kJ mol^{-1}) than B3LYP/LANL2DZP($\Delta E = -54.4$ kJ mol^{-1}) does, in accordance with findings for weak Si···N interactions (H. Fleischer, *Eur. J. Inorg. Chem.*, 2001, 393).
31 T. B. Brill and N. C. Campbell, *Inorg. Chem.*, 1973, **12**, 1884.